Influences of Using Different Satellite Soil Moisture Products on SM2RAIN for Rainfall Estimation Across the Tibetan Plateau

Linguang Miao, Zushuai Wei, Fengmin Hu, and Zheng Duan

***Abstract*—The SM2RAIN (soil moisture to rain) model has been widely used for rainfall estimation worldwide. However, due to the lack of sufficient ground observation, the SM2RAIN model driven by different passive microwave soil moisture products over the Tibetan Plateau has not been fully validated. In this article, four widely used satellite microwave soil moisture products (including SMAP, ASCAT, SMOS, and AMSR2) were used as input data for rainfall estimation. Rainfall data from eight ground observation stations during 2016–2018 were used to evaluate the overall performance of the SM2RAIN algorithm under various soil moisture products at different time aggregation scales. In addition, different satellite soil moisture products were merged to evaluate whether the combined soil moisture products could improve the performance of the SM2RAIN model. Finally, the rainfall estimates with different soil moisture data were further evaluated and compared with two benchmark rainfall products (IMERG and ERA5). Results indicate that: 1) Overall, SM2RAIN-SMAP has the highest rainfall estimation accuracy, but with the time aggregation scale up to 30 days, the mean *R* of the four rainfall estimates could reach above 0.8 and the mean value of Kling–Gupta efficiency could reach above 0.8. 2) Combined satellite soil moisture products can significantly improve the rainfall estimates. The SM2RAIN model performed the best when SMAP and ASCAT soil moisture products were combined. 3) Using the SMAP product or combined soil moisture products yielded more accurate rainfall estimates than the two benchmark rainfall products (IMERG and ERA5).**

***Index Terms*—AMSR2, ASCAT, rainfall estimation, SM2RAIN, SMAP, SMOS, soil moisture.**

I. Introduction

RAINFALL is an important variable of the global water and energy cycle [1], [2], [3] and is also the main driver of the hydrological and land surface processes [4]. Rainfall directly influences the spatial and temporal evolution of hydrological cycle components such as runoff, soil moisture, and evapotranspiration. In addition, extreme rainfall events usually trigger flood disasters, mountain landslides [5], [6], [7], [8]. In the past three decades, the warming and humidification trend over the Tibetan Plateau has intensified [9], [10], [11], [12], and the time, frequency, and intensity of regional rainfall have changed significantly [13], [14]. Improving rainfall monitoring capability is of great significance for drought monitoring, flood disaster warning, and water resource management in the Tibetan Plateau.

Conventional rainfall observation mainly relies on in situ stations [15], using local point sampling to represent true rainfall over tens or even hundreds of square kilometers [16], [17]. in situ measurement can ensure high accuracy but is limited by the uneven distribution of ground sensors, while the rainfall information is only available for certain parts of the region [18]. Meteorological and hydrological processes mutually affect each other at global and local scales. The linkage between meteorological variables with hydrological variables at a local scale is expected to vary both with time and space. Due to its continuously evolving characteristics, and such interactions or associations are difficult to model [19], [20], [21], [22]. Remote sensing provides a new technique for detecting the spatial and temporal distribution and rainfall change in a large area. Compared with ground observation, satellite observation has the advantage of spatial continuity and can provide rainfall information in areas without observation data. The continuous updating and improvement in rainfall remote sensing techniques provide an important tool for estimating rainfall at the global scale. Satellite rainfall products have gradually become an important data source in the hydrometeorological field [23], [24].

Recently, a state-of-the-art method named SM2RAIN was proposed [25] to directly estimate rainfall by using dynamic changes in soil moisture. SM2RAIN is a bottom-up rainfall estimation method based on the soil water balance equation. It can capture the rainfall event that occurred between two soil moisture observations. Currently, the SM2RAIN method has been evaluated and applied using different satellite soil moisture data over different regions worldwide. Subsequent versions of the algorithm, toward more independent [24] and rigorous [26], have been proposed. Related rainfall products such as

Manuscript received 30 March 2023; revised 24 May 2023 and 5 July 2023; accepted 12 July 2023. Date of publication 18 July 2023; date of current version 2 August 2023. This work was supported in part by the Guangdong Basic and Applied Basic Research Foundation under Grant 2020A1515110507, and in part by The Crafoord Foundation under Grant 20200595 and Grant 20210552. *(Corresponding authors: Zushuai Wei; Zheng Duan.)*

Linguang Miao is with the School of Surveying and Land Information Engineering, Henan Polytechnic University, Jiaozuo 454150, China (e-mail: miaolinguang@home.hpu.edu.cn).

Zushuai Wei is with the School of Artificial Intelligence, Jianghan University, Wuhan 430056, China (e-mail: weizushuai@scies.org).

Fengmin Hu is with the College of Surveying and Geo-Informatics, North China University of Water Resources and Electric Power, Zhengzhou 450046, China (e-mail: hufengmin@ncwu.edu.cn).

Zheng Duan is with the Department of Physical Geography and Ecosystem Science, Lund University, S-22362 Lund, Sweden (e-mail: zheng.duan@nateko.lu.se).

Digital Object Identifier 10.1109/JSTARS.2023.3296455

SM2RAIN-CCI (the European Space Agency Climate Change Initiative) and SM2RAIN-ASCAT (the Advanced Scatterometer) have been developed and released [27], [28], [29]. The validation practice also reveals the good potential of SM2RAIN in cumulative rainfall estimation [29]. Different studies have explored the practical value of these products for hydrological applications such as drought monitoring [30] and landslide prediction [31].

Although many studies have demonstrated the SM2RAIN algorithm's good performance, its uncertainty is also worthy of attention. The SM2RAIN algorithm captures rainfall through the dynamic change of soil moisture, and the reliability of rainfall estimation depends on the accuracy of input soil moisture data. Existing studies have shown that passive microwave soil moisture products have high accuracy [32], [33], [34], [35], [36], [37], especially SMAP satellite equipped with L-band passive microwave radiometer is considered to be able to provide excellent soil moisture products.

The performance of the SM2RAIN algorithm can vary significantly in different regions due to variations in soil moisture inputs. For instance, in India, both SM2RAIN-ASCAT and SM2RAIN-SMAP exhibit similar performance, whereas in Italy, SM2RAIN-ASCAT outperforms SM2RAIN-SMAP [38]. Additionally, the estimation of passive microwave soil moisture in mountainous areas remains uncertain, posing challenges to the application of the SM2RAIN algorithm in such regions. The Tibetan Plateau, in particular, is characterized by complex topography and uneven spatial distribution of rainfall. Due to limited availability of ground data, the evaluation of SM2RAIN in the Tibetan Plateau has been restricted. Moreover, the performance differences among widely used satellite soil moisture products, including SMAP, ASCAT, SMOS, and AMSR2, as input data for the SM2RAIN method, are not well understood over the Tibetan Plateau.

The objectives of this study are as follows.

1) To evaluate the performance of four satellite soil moisture products, SMAP, ASCAT, SMOS, and AMSR2, respectively, as input data of the SM2RAIN algorithm in the Tibetan Plateau.
2) To combine different satellite soil moisture products to improve the performance of the SM2RAIN algorithm.
3) To compare the performance of SM2RIAN-ASCAT rainfall products, IMERG satellite rainfall products and ERA5 reanalysis rainfall products, and the regional calibrated SM2RAIN rainfall estimation.

The article is organized into five sections. Following the Introduction, Sections II and III describe the study area and datasets, and methodology, respectively. Section IV highlights the results. The discussion and conclusion are presented in Sections V and VI, respectively.

II. Study Area and Datasets

A. Study Area

The Tibetan Plateau is the highest plateau in the world, with an average elevation of more than 4000 meters. The terrain is high in the northwest and low in the southeast, and slopes from northwest to southeast (see Fig. 1). We used the DEM data source of ASTER GDEM V2 (https://earthexplorer.usgs.gov). The Tibetan Plateau is a typical alpine climate region. The annual precipitation is about 500 mm, and the regional climate is mainly influenced by the westerly winds, the South Asian monsoon, and the East Asian monsoon circulation [7]. Its summer is cool and rainy, winter is dry and cold, with less rain, the temperature difference between day and night is big. The spatial distribution of rainfall gradually decreased from southeast to northwest [39], this is consistent with the distribution characteristics of different climatic regions in the Tibetan Plateau. In addition, there are noticeable seasonal fluctuations in the rainfall over the Tibetan Plateau, primarily from May to September [40]. The predominant form of land cover is meadow [41]. Fig. 1 depicts the terrain and location of meteorological stations on the Tibetan Plateau.

B. Ground-Based Observed Data

Rainfall over the Tibetan Plateau has significant spatial variability and seasonal characteristics [39]. Ground rainfall observation data were obtained from National Tibetan Plateau Data Center (https://www.tpdc.ac.cn/zh-hans) [42]. This study used eight rainfall observation sites from 2016 to 2018 (see Table I). These stations cover different climatic regions with significant differences in vegetation coverage conditions, which represent the climatic conditions and vegetation growth of the Tibetan Plateau. Land cover type information is obtained from rain gauge site statistics. Since alpine meadow and alpine grassland have similar performance, we discuss them together when analyzing different land cover types.

To validate the suitability of the SM2RAIN method for the Tibetan Plateau, we have included in situ soil moisture data from the Ali and Naqu stations [43]. The in situ soil moisture observations were collected from stations located near the rain gauges. The temporal resolution of the in situ soil moisture data is 15 minutes. To match the one-day resolution of the rain gauge data, we aggregated the in situ soil moisture measurements to a one-day sampling interval using arithmetic mean method.

There is a scale mismatch between the ground stations and the corresponding satellite pixels. The ground sites can only represent a limited area around them and may not accurately reflect the larger scale conditions. However, our focus in this study is on comparing different rainfall data rather than conducting absolute accuracy validation. It is worth noting that all four satellite soil moisture products used in our analysis are subject to this scale effect. While this may impact the accuracy of rainfall estimation, it does not significantly affect the comparison of rainfall estimation among the four satellite soil moisture products.

C. Remotely Sensed Soil Moisture Products

The satellite soil moisture and rainfall data used in this study are shown in Table II.

The SMAP radiometer can provide soil moisture observations at a resolution of 36 km with a revisit period of 2–3 days [44]. SMAP satellite has four levels of data products, including level

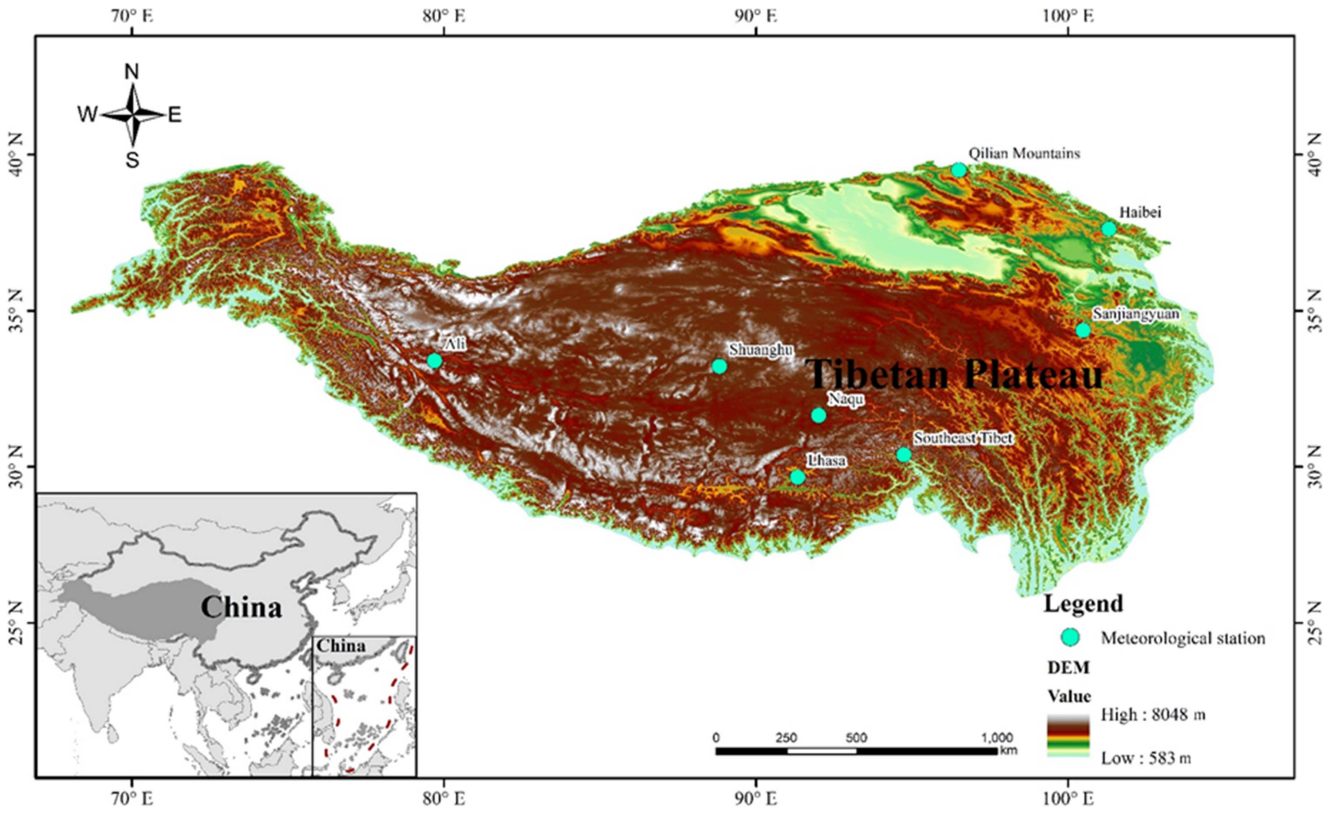

Fig. 1. Topographic map and distribution of meteorological stations over the Tibetan plateau.

TABLE I
INFORMATION ABOUT THE GROUND OBSERVATION STATIONS USED IN THIS STUDY

Sym	Station	Longitude (°E)	Latitude (°N)	Frequency	Land Cover	Altitude(m)
S1	Southeast Tibet	94.74	30.3833	Daily	Forest	3326
S2	Lhasa	91.33333	29.66667	Daily	Artificial grass	3688
S3	Ali	79.70133	33.39167	Daily	Desert	4264
S4	Haibei	101.3167	37.61667	Daily	Alpine meadow	3220
S5	Sanjiangyuan	100.4833	34.37	Daily	Alpine meadow	3958
S6	Qilian Mountains	96.5	39.5	Daily	Alpine meadow	4200
S7	Naqu	92.0097	31.6437	Daily	Alpine meadow	4602
S8	Shuanghu	88.83223	33.2167	Daily	Alpine grassland	6055

TABLE II
LIST OF SATELLITE SOIL MOISTURE PRODUCTS AND RAINFALL PRODUCTS USED IN THIS STUDY

Abbreviations of the dataset	Data Type	Spatiotemporal resolution	Period covered in time
SMAP	SM	36km	2015 to present
ASCAT(H119)	SM	12.5km	2007–2020
SMOS	SM	25km	2010 to present
ASMR2	SM	0.25°	2012 to present
ESA CCI	SM	0.25°	1978–2021
SM2RAIN-ASCAT	Rainfall	0.125°	2007–2022
ERA5	Rainfall	0.25°	1950 to present
IMERG-Late	Rainfall	0.1°	2000 to present

L1 sensor observation data, level L2 single-orbit soil moisture data, level L3 multiorbit daily composite soil moisture data, and level L4 assimilation products, all data products are projected onto the EASE-2 Grid (Equal-Area Scalable Earth grid ver. 2). These products are available through the NASA National Snow and Ice Data Center Distributed Active Archive Center, NSIDC DAAC) (https://ladsweb.modaps. eosdis.nasa.gov/) for free. Here, we use surface soil moisture (0–5 cm) data from SMAP Level-3 Version 8, with a period of 2016–2020.

The Advanced scatterometer (ASCAT) is a scatterometer mounted on the meteorological service Metop-A, B, and C. We use a soil moisture product (H119) provided under the European organization for the exploitation of the METeorological SATellites (EUMETSAT) program. The soil moisture data were obtained by retrieval of the backscattering coefficients observed by the ASCAT scatterometer using the change detection algorithm described in paper [45]. The spatial resolution of the data is 12.5 km. The temporal resolution depends on the latitude and number of MetOp satellites used (http://hsaf.meteoam.it/).

SMOS (the soil moisture ocean salinity) satellite, launched in 2009, is specially designed to detect surface moisture and ocean salinity. The satellite is equipped with the synthetic aperture microwave imaging radiometer (MIRAS), which operates in the microwave L band and is the first space-based two-dimensional interference radiometer operating in a polar orbit. In this study, the recently released SMOS-IC v2 product (https://ib.remotesensing.inrae.fr/) was selected. The SMOS-IC product has a spatial resolution of 25 km and daily soil moisture data for ascending and descending orbits [46].

The AMSR2 sensor was deployed on the Global Change Observation Mission 1-Water (GCOM-W1) satellite, which was launched in May 2012 [47]. It has the capability to provide global land observations twice daily through ascending and descending orbits [48]. The primary spatial resolution of the AMSR2 dataset is defined by 0.25° global grids. For soil moisture retrieval, the AMSR2 employs two main algorithms: the land parameter retrieval model and the Japan Aerospace Exploration Agency algorithm [49], [47].

ESA CCI soil moisture dataset version 7.1 was used in this study. The SM dataset has three products, namely active microwave data, passive microwave data, and their combination. A combination product was used in this study [50], [51].

A comprehensive evaluation of the satellite soil moisture data was conducted, and rigorous data quality checks were implemented, resulting in the exclusion of data with poor quality information. Furthermore, special consideration was given to the influence of seasonal frozen soils by incorporating the mask information provided within the satellite soil moisture data. Specifically, during periods characterized by seasonal frozen conditions, the corresponding data were carefully removed to ensure the integrity of the analysis, free from any potential biases introduced by these specific circumstances.

D. Rainfall Products

In this study, we used three rainfall products, SM2RAIN-ASCAT, ERA5, and IMERG-Late.

SM2RAIN-ASCAT is a new global-scale rainfall product obtained by using ASCAT soil moisture data based on the SM2RAIN algorithm [29]. The spatial resolution of SM2RAIN-ASCAT is 0.125° × 0.125°, and the temporal resolution is 1 day. SM2RAIN-ASCAT data is available from 2007 to 2022 (https://zenodo.org/record/7950103).

ERA5 is the latest generation of global reanalysis datasets produced by the European Centre for Medium-Range Weather Forecasts (ECMWF), providing dozens of commonly used surface and atmospheric variables covering the period from 1950 to the present [52]. By assimilating a large number of ground observations, atmospheric sounding data, and remote sensing data, ERA5 provides reasonable spatio-temporal variability of large-scale precipitation. The spatial resolution of ERA5 reanalysis precipitation data is 0.25° × 0.25°, and the temporal resolution is 1 hour.

IMERG (integrated multisatellite retrievals for GPM) is a new generation of multisatellite joint precipitation retrieval products planned by GPM (global precipitation measurement). IMERG combines space-borne microwave, infrared, rainfall radar, and other sensors to realize the complementary advantages of multiple data sources. IMERG precipitation product was first released at the beginning of 2015 with a spatial resolution of 0.1° × 0.1° and a temporal resolution of 0.5 hours [53]. The rainfall data of the IMERG-Late version was used in this study.

III. Methodology

A. SM2RAIN Algorithm

On the basis of the soil water balance equation, the SM2RAIN algorithm can directly estimate the accumulated rainfall between the two-time intervals by using the change information of soil moisture [25]. The soil water balance equation for the soil water capacity Z (L) can be described by the following expression:

$$Zds\,(t)/dt = p\,(t) - r\,(t) - e\,(t) - g\,(t) \tag{1}$$

where $s(t)$ (-) is the relative saturation of the soil or relative soil moisture, t *(d)* is the time and $p(t)$, $r(t)$, $e(t)$, and $g(t)$ (mm/d) are the precipitation, surface runoff, evapotranspiration, and drainage rate, respectively [27]. Whenever it rains, the evaporation rate can be safely assumed as negligible ($e(t) = 0$). Moreover, by assuming that all precipitation infiltrates into the soil, the runoff rate is zero ($r(t) = 0$). For the drainage rate, the following relation may be adopted, $g(t) = as(t)^b$, where a (mm/d) is the saturated hydraulic conductivity, b is the exponent related to the pore size distribution index [54]. Rearrange formula (1) according to the hypothesis, rainfall can be estimated from the following equation:

$$p\,(t) \cong \frac{Zds\,(t)}{dt} + as(t)^b. \tag{2}$$

Through (2), cumulative rainfall can be estimated using relative soil moisture or soil relative saturation and its temporal fluctuation $ds(t)/dt$, as well as three corrected parameters (Z, a, b).

B. Three-Dimensional Discrete Cosine Transform

In this article, the discrete cosine transform—penalty least squares (DCT-PLS) method is used to fill the missing values of satellite soil moisture products. DCT-PLS is a smoothing algorithm [55], [56], [57]. PLS regression smooths the original data by minimizing (3), which consists of a residual term between the original data and the smooth data and a penalty term for the roughness of the smooth data. To reconstruct and complete SM soil moisture products (θ), a multidimensional robust smooth regression algorithm was applied

$$F\left(\hat{\theta}\right) = \text{RSS} + s\text{PT}\left(\hat{\theta}\right) = \left\|\hat{\theta} - \theta\right\|^2 + s\text{PT}\left\|\hat{\theta}\right\|. \quad (3)$$

Among them, θ, RSS, PT, and s are soil moisture, sum of residual squares, penalty term, and actual positive parameter, respectively, which are used to control the degree of smoothing function (F). $\|\|$represents the Euclidean norm, for multidimensional data, DCT can be used to represent PLS, so DCT-PLS can be spatially applied to fill the gaps in the grid data

$$F\left(\hat{\theta}\right) = \left\|W^{1/2} \circ \left(\hat{\theta} - \theta\right)\right\|^2 + s\left\|\Delta\hat{\theta}\right\| \quad (4)$$

where $\circ$ and Δ representative and missing and available data of θ_i elements product and Laplacian, W is a binary array with the same size, indicating whether or not the lack of value. For more information on mathematical reasoning processes, see paper [55].

C. Combining Different Soil Moisture Products

In this study, two different soil moisture combination methods were used to evaluate the impact of combined soil moisture data on the SM2RAIN algorithm. Considering the systematic errors between different soil moisture products [58], in the first method, the conversion between different satellite soil moisture products takes one soil moisture product as a reference to eliminate the systematic errors of the other one [26], [59] and the conversion formula can be expressed as follows:

$$\text{SM}_{\text{normalized}} = (\text{SM}_1 - \mu_{\text{SM}_1}) \times \frac{\sigma_{\text{SM}_2}}{\sigma_{\text{SM}_1}} + \mu_{\text{SM}_2}. \quad (5)$$

In this equation, SM_1 is the soil moisture product to be calibrated, SM_2 is the reference soil moisture product, μ and σ represent the mean and variance of soil moisture products, respectively. $\text{SM}_{\text{normalized}}$ is the soil moisture product after the systematic error is eliminated. Then, the average value between the corrected two soil moisture products and the reference soil moisture products is calculated as the combined soil moisture data of the input of the SM2RAIN algorithm:

$$\text{SM}_{\text{mean}} = \frac{\text{SM}_{\text{normalized}} + \text{SM}_2}{2} \quad (6)$$

where SM_{mean} is the combined soil moisture.

The second combination method was summed by assigning different weights to the two soil moisture products [47], [60]

$$\text{SM}_{\text{com}} = \omega \times \text{SM}_1 + (1 - \omega)\,\text{SM}_2\,(0 \le \omega \le 1) \quad (7)$$

where SM_{com} is the combined soil moisture, and ω is the weight. In this article, ω is also used as a parameter to be calibrated together with Z, a and b when combining different soil moisture.

D. Performance Metrics

In this study, the SM2RAIN model was calibrated using in situ rainfall observations and SMAP soil moisture products from 2016 to 2017, while the performance of model-derived rainfall estimation was evaluated using data from 2018. Five performance metrics were used to evaluate the SM2RAIN model, including Pearson's Correlation (R), Kling–Gupta efficiency (KGE), Nash-Sutcliffe efficiency index (NS), root mean squared error (RMSE), and Bias (see Table III). Where R ranges in value $(-1, 1)$, representing the correlation between observations and estimates. The KGE ranges in value $(-\infty, 1)$, representing the robustness between observations and estimates. The NS ranges $(-\infty,1)$, indicate the overall performance. The closer it is to 1, the model is more accurate and reliable. The RMSE is used to characterize the estimation error, where the closer the value is to 0, the better the estimation. The BIAS represents the deviation between the estimates and the observations value. If the value is less than 0, the model underestimates the observed value; if the value is greater than 0, the model overestimates the observed value.

IV. Results

A. Rainfall Estimation Using in situ Soil Moisture

The SM2RAIN algorithm was initially proposed in Italy, situated in southern Europe [25]. Extensive ground validation has consistently demonstrated the algorithm's strong performance in estimating rainfall [25]. Furthermore, empirical investigations involving in situ soil moisture derived rainfall estimations in alpine mountainous areas have consistently confirmed the algorithm's suitability for such terrains [61], [62]. Notably, SM2RAIN has released comprehensive global products [28], [29], encompassing the vast expanse of the Tibetan Plateau. To assess the suitability of the SM2RAIN algorithm for the Tibetan Plateau, two representative soil moisture stations, Ali and Naqu, were employed to estimate rainfall (see Fig. 2). We use 2016 data calibration and 2017 data validation. There is a good correlation between the rainfall results estimated by Ali station and the rain gauge (Calibration $R = 0.767$; Validation $R = 0.639$) [see Fig. 2(a) and (b)] The correlation of Naqu station during the calibration period is relatively poor (Calibration $R = 0.451$; Validation $R = 0.633$), but good during the validation period [see Fig. 2(c) and (d)]. This may be due to regional differences in the distribution of rain gauges and in situ soil moisture sensors. It may also be due to the inability of in situ sampling intervals to respond well to changes in soil moisture caused by rainfall. High-frequency in situ soil moisture and rain gauge observations may improve the performance of the SM2RAIN algorithm.

The analysis of rainfall estimation using in situ soil moisture has demonstrated that the SM2RAIN algorithm is capable of consistently reproducing accumulated rainfall, even when faced with limited observation times. This finding holds significant

TABLE III
EQUATIONS USED FOR THE PERFORMANCE METRICS

Performance score	Score symbol	Equation
Pearson's Correlation	R	$R = \frac{\mathrm{cov}(X_{obs}, X_{sim})}{\sigma(X_{obs})\sigma(X_{sim})}$
Kling-Gupta Efficiency	KGE	$KGE=1-\sqrt{(1-R)^2+\left(1-\frac{\mu(X_{sim})}{\mu(X_{obs})}\right)^2+\left(1-\frac{\sigma(X_{sim})/\mu(X_{sim})}{\sigma(X_{obs})/\mu(X_{obs})}\right)^2}$
Nash-Sutcliffe Efficiency	NS	$NS=1-\sqrt{\frac{\sum(X_{obs}-X_{sim})^2}{\sum(X_{obs}-\overline{X_{obs}})^2}}$
Bias	BIAS	$BIAS=\frac{\sum(X_{sim}-X_{obs})}{N}$
Root Mean Squared Error	RMSE	$RMSE=\sqrt{\frac{\sum(X_{obs}-X_{sim})^2}{N}}$

Note: Where X_{obs} is the observed value; X_{sim} is the estimated value; cov is the covariance operator, μ is the mean operator, σ is the standard deviation operator, $\sum$ is the summation operator; N is the sample size, $\overline{X_{obs}}$ is the mean of the observed values.

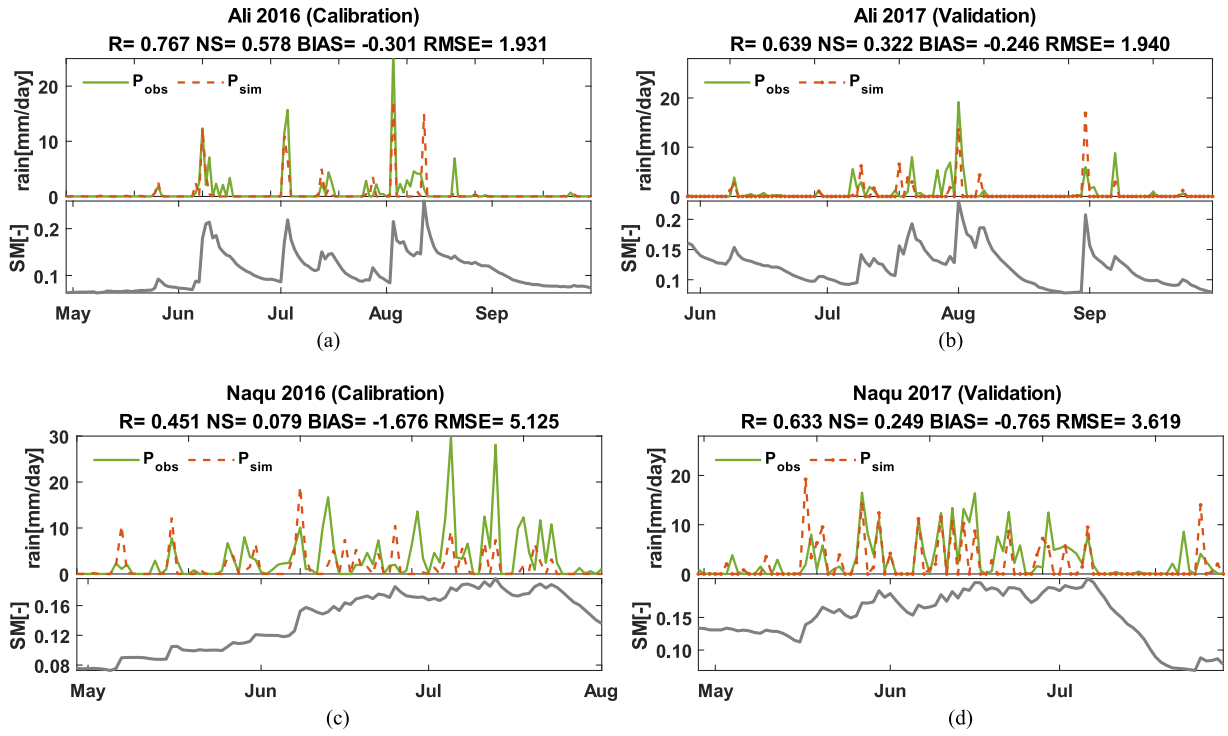

Fig. 2. Rainfall time series curves of in situ soil moisture estimation at Ali and Naqu stations.

implications, as it provides valuable support for utilizing satellite soil moisture data to estimate rainfall over the Tibetan Plateau.

B. Rainfall Estimation Using Different Soil Moisture Products

Fig. 3 displays how the SM2RAIN algorithm performs when SMAP, SMOS, AMSR2, and ASCAT soil moisture products are utilized as input data, respectively. Time series *R* and *KGE* at each site were used to evaluate the robustness of the SM2RAIN algorithm for rainfall estimation [see Fig. 3(a)]. For both the calibration and validation period, most sites show a gradual improvement in the performance of the SM2RAIN algorithm, with the increase of AGGR. The *R* and *KGE* with AGGR of 7, 14, and 30 days is significantly better than that with AGGR of 1 day. When AGRR is 7, the growth of various performance metrics tends to slow down and reach a relatively stable level. In the calibration and validation periods, stations S6 and S7 located in the central semi-arid region of the Tibetan Plateau achieved the highest correlation between estimated and observed values in four different AGGR values, indicating the superior performance of the SM2RAIN algorithm in the semi-arid region [30]. The *R* values were slightly lower in the validation period than in the calibration period but remained >0.7 for all sites with AGGR equal to 7, 14, and 30. Similarly, KGE performed

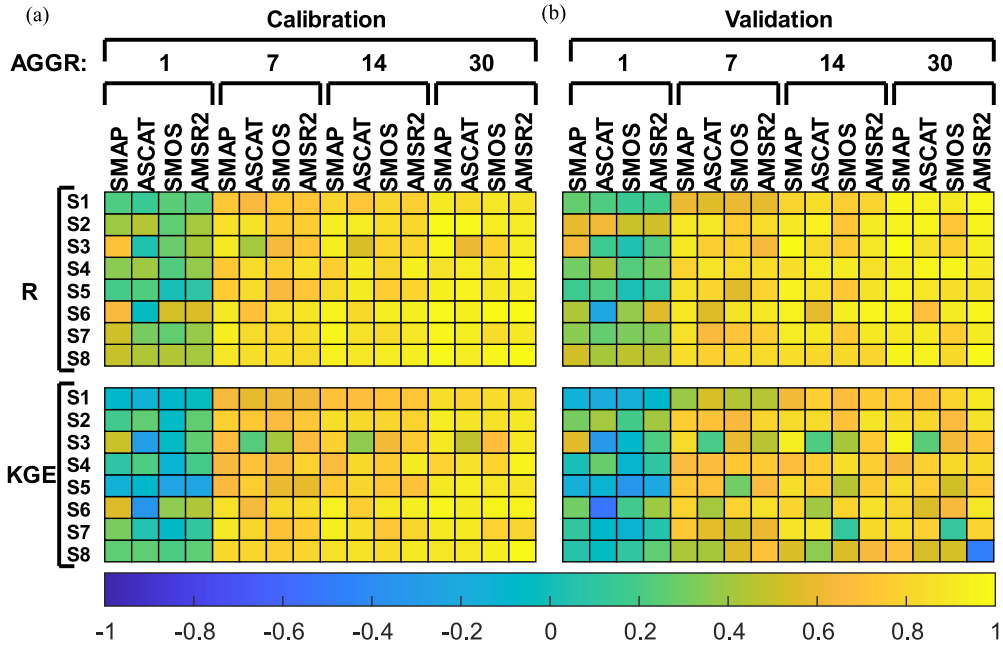

Fig. 3. Performance of SM2RAIN using SMAP, ASCAT, SMOS, and AMSR2 soil moisture product at different stations for AGGR = 1, 7, 14, and 30. (a) *R* and KGE values for calibration period. (b) *R* and KGE values for the validation period.

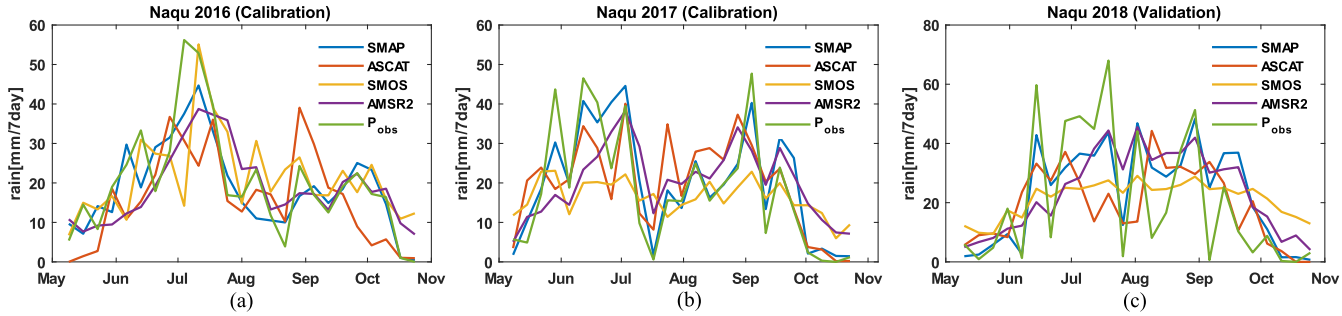

Fig. 4. Rainfall time series curves of soil moisture estimation from different satellites at Naqu Station.

better during the calibration period compared to the validation period, especially when AGGR was 14 and 30. In AGRR > 7, the KGE of most sites is greater than 0.6. Under the same conditions of AGGR and satellite soil moisture products, the KGE performance of S6, S7, and S8 stations is the highest. Rainfall estimates based on SMAP soil moisture data showed higher *R* and KGE values at the same AGRR and sites.

Fig. 4 shows the rainfall estimation results of four kinds of satellite soil moisture at Naqu station with a time step of 7 days. The four satellite soil moisture estimation rainfall results can capture the temporal variation of the rain gauge. Although there are some places where the rainfall is overestimated or underestimated, it is generally consistent with the rain gauge.

To further quantitatively elucidate the differences in the performance of the SM2RAIN algorithm under different AGGR and various satellite soil moisture products, we investigate the mean values of the performance metrics of the SM2RAIN algorithm based on different soil moisture products at all stations in the calibration and validation periods in Fig. 5. The trend of mean *R* of rainfall estimation accompanied by AGGR was basically the same in the validation and calibration periods, and the mean *R* in the validation period were lower than those in the calibration period, but the decrease did not exceed 5%. The mean *R* of SM2RAIN-SMAP and SM2RAIN-AMSR2 rainfall estimation showed better performance. In the calibration period, the mean R of AGGR for 7 days was larger than 0.8, and the mean R of AGGR for 30 days was larger than 0.9 [see Fig. 5(a)]. Similarly, the mean KGE values of SM2RAIN-SMAP and SM2RAIN-AMSR2 rainfall estimates performed better [see Fig. 5(b)], and the mean KGE value for AGGR of 30 days was also greater than 0.9. However, the algorithms did not perform as well in the validation period as in the calibration period, and the mean KGE values of the four rainfall estimates in the validation period decreased by 9%–25% compared to the calibration period at an AGGR of 30 days.

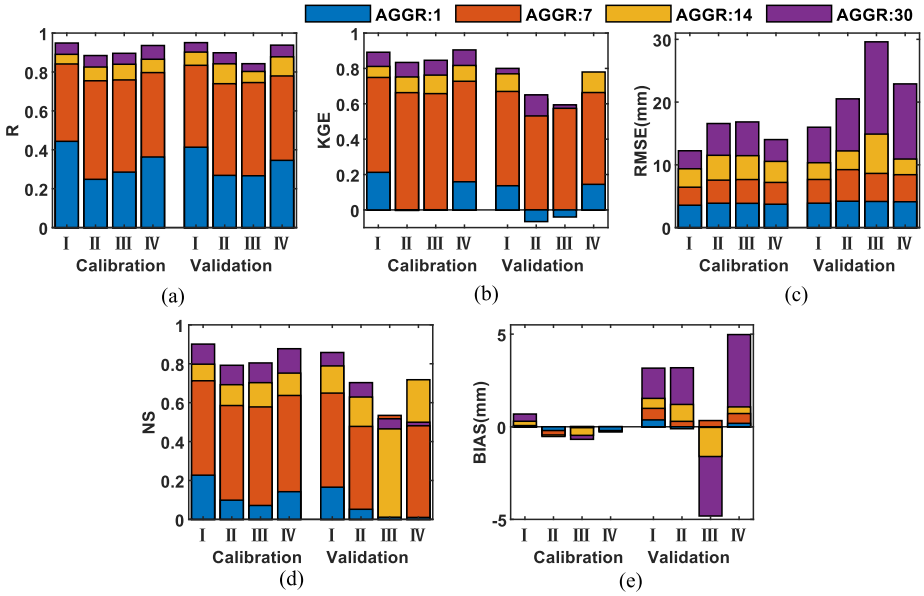

Fig. 5. Performance of four different rainfall estimates in AGGR 1, 7, 14, and 30. (a), (b), (c), (d), and (e), respectively, represent the mean values of R, KGE, RMSE, NS, and BIAS of all sites. (I stands for SM2RAIN-SMAP, II for SM2RAIN-ASCAT, III for SM2RAIN-SMOS, IV for SM2RAIN-AMSR2).

The four rainfall estimates performed significantly better than the validation period in terms of mean RMSE, mean NS and mean BIAS in the calibration period [see Fig. 5(c)–(e)]. The mean RMSE values of rainfall estimates were all about 4 mm at an AGGR of 1 day (calibration and validation periods), but as the AGGR increased, the mean RMSE values became larger with it, which may be due to the accumulation of multiday errors. Among the four satellite soil moisture products, the mean RMSE values of SM2RAIN-SMAP rainfall estimation were the lowest at AGGR of 7, 14, and 30 days. During the calibration period, SM2RAIN-AMSR2 had the second-highest RMSE after SM2RAIN-SMAP, and SM2RAIN-SMOS and SM2ASCAT performed similarly. However, during the validation period, the RMSE of SM2RAIN-ASCAT is closer to that of SM2RAIN-SMAP, the RMSE of SM2RAIN-AMSR2 is slightly larger, and the RMSE of SM2RAIN-SMOS is the largest. The relatively good performance obtained by SM2RAIN-AMSR2 may be related to the use of a more robust missing value-filling algorithm for the AMSR2 soil moisture data in this article [63]. The poor performance of SM2RAIN-SMOS may be caused by the fact that SMOS soil moisture is severely affected by radio frequency interference (RFI) in the Tibetan Plateau region, resulting in poor accuracy of soil moisture retrieval [64], [65]. In terms of NS, similar to what RMSE shows, SM2RAIN-SMAP is the best ($\sim$0.85) and SM2RIAN-SMOS is the worst (no more than 0.6). In the calibration period, the mean value of BIAS is close to 0. In the validation period, when the AGGR is 30, the mean values of BIAS for SM2RAIN-SMAP, SM2RAIN-ASCAT and SM2RAIN-AMSR2 are greater than 3 mm, showing an overestimation of rainfall. Among them, SM2RAIN-AMSR2 has the largest overestimation. SM2RAIN-SMOS, on the contrary, has a mean BIAS value of about -5 mm and exhibits underestimated rainfall. Overall, the SMAP soil moisture product achieves the highest accuracy when used as input data for the SM2RAIN algorithm, which is consistent with previous validation work on satellite soil moisture products in the Tibetan Plateau [66], [67], [68], indicating that the quality of the SM input significantly influences the performance of the SM2RAIN algorithm.

C. Rainfall Estimation on Different Land Covers

Fig. 6 compares the performance of the four rainfall estimates under different land cover types (land cover types are determined according to the latitude and longitude where the stations are located.) The performance of the four rainfall product estimates varies across land cover types. Under all land cover types, R and KGE basically follow the pattern of improving performance as AGGR increases. Compared with the calibration period, the value of R did not decrease significantly in the validation period, but KGE showed different magnitudes of decrease under different land cover types.

During the calibration period, the performance of the SM2RAIN-ASCAT estimated rainfall under Forest was lower relative to the other rainfall estimates, and the R and KGE of the SM2RAIN-ASCAT rainfall estimates were lower than the other rainfall estimates [see Fig. 6(a) and (b)]. The BIAS of the SM2RAIN-ASCAT rainfall estimates was about -5 mm, which exhibited a significant underestimation of rainfall compared to the other three rainfall estimates. However, during the validation period, the *BIAS* of all four rainfall estimates was larger than 0 mm, showing an overestimation of rainfall, especially when the AGGR was 30 days, and the *BIAS* of SM2RAIN-SMAP and SM2RAIN-ASCAT was about 10 mm [see Fig. 6(c)].

Taking AGGR as an example for 1 day, the R and KGE of SM2RAIN-SMOS under Grassland were 0.26 and -0.05 (calibration period), respectively, which were significantly lower than the R ($>$0.4) and *KGE* ($>$0.18) of the other three rainfall estimates [see Fig. 6(a) and (b)]. A similar

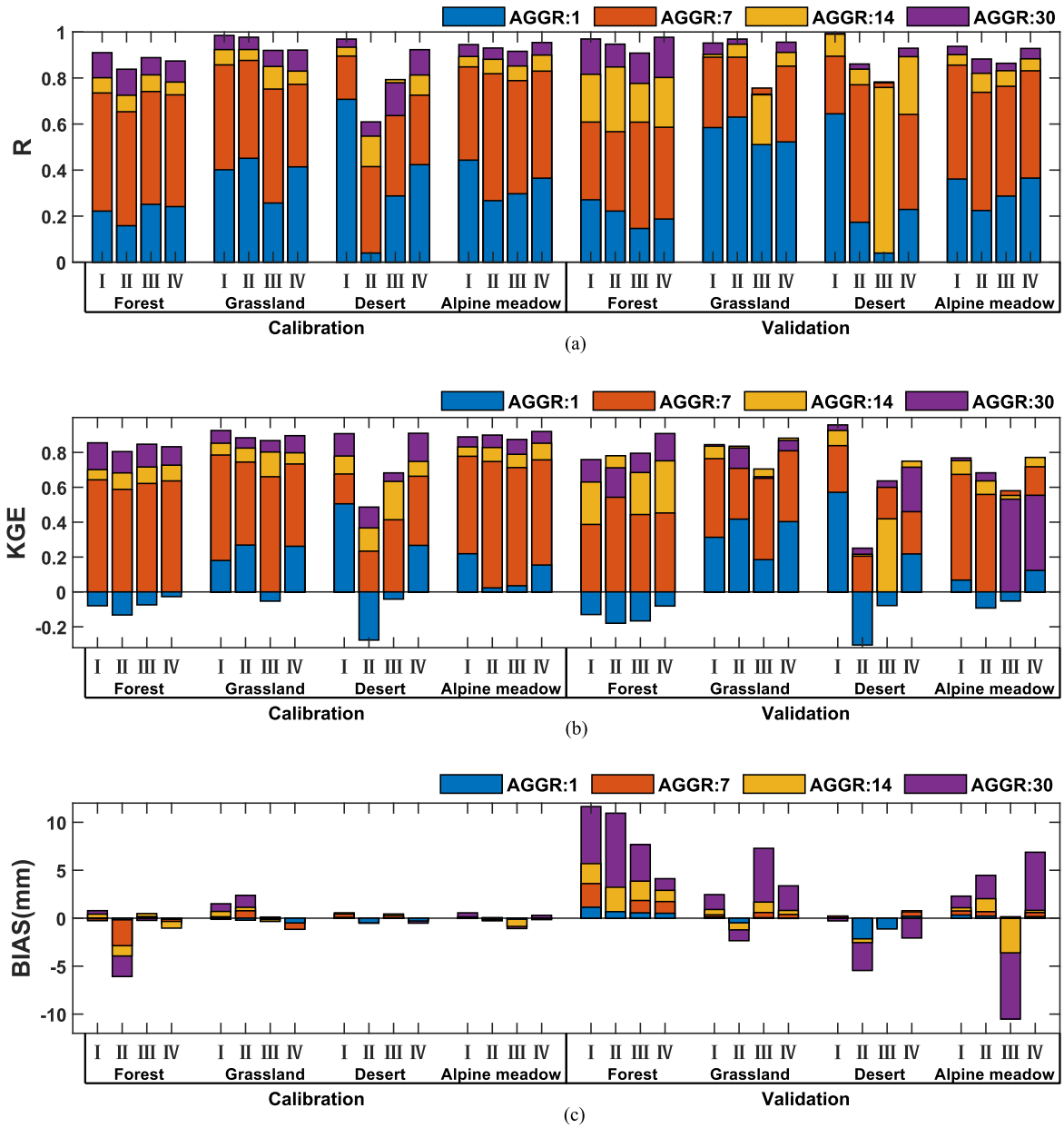

Fig. 6. Evaluation metrics (*R*, KGE, and BIAS) for SM2RAIN-SMAP, SM2RAIN-ASCAT, SM2RAIN-SMOS, and SM2RAIN-AMSR2 rainfall estimates under four land covers. (I stands for SM2RAIN-SMAP, II for SM2RAIN-ASCAT, III for SM2RAIN-SMOS, IV for SM2RAIN-AMSR2).

performance was shown in the validation period, where *R* and *KGE* of SM2RAIN-SMOS were lower than the other three rainfall estimates. In Alpine meadow, SM2RAIN-SMAP and SM2RAIN-AMSR2 performed better than SM2RAIN-ASCAT and SM2RAIN-SMOS during the calibration and validation periods [see Fig. 6(a) and (b)].

It can be clearly seen that SM2RAIN-SMAP under Desert has the best performance of *R* (0.71) and KGE (0.51) (calibration period when AGGR is 1 day). Similarly, *R* (0.64) and KGE (0.57) of SM2RAIN-SMAP were significantly better than the other three rainfall estimates during the validation period.

Overall, SM2RAIN-SMAP demonstrated excellent performance in rainfall estimation across all four land cover types, particularly in the Desert region. Meanwhile, SM2RAIN-ASCAT exhibited superior performance in Grassland areas. SM2RAIN-SMOS rainfall estimation in four land covers has no significant advantage over other rainfall estimations, but *R* and KGE can maintain better accuracy with increasing AGGR.

The performance of the SM2RAIN algorithm exhibits significant regional variations due to the different soil moisture inputs [38]. We hypothesize that the favorable performance of SM2RAIN-SMAP in desert regions may be attributed to the greater penetration depth of L-band data from SMAP, allowing for a more accurate representation of soil moisture changes [69], [70]. Similarly, the improved performance of SM2RAIN-ASCAT in grassland areas may be attributed to ASCAT's higher temporal coverage and reduced influence of the DCT-PLS algorithm. However, it is important to note that further validation is

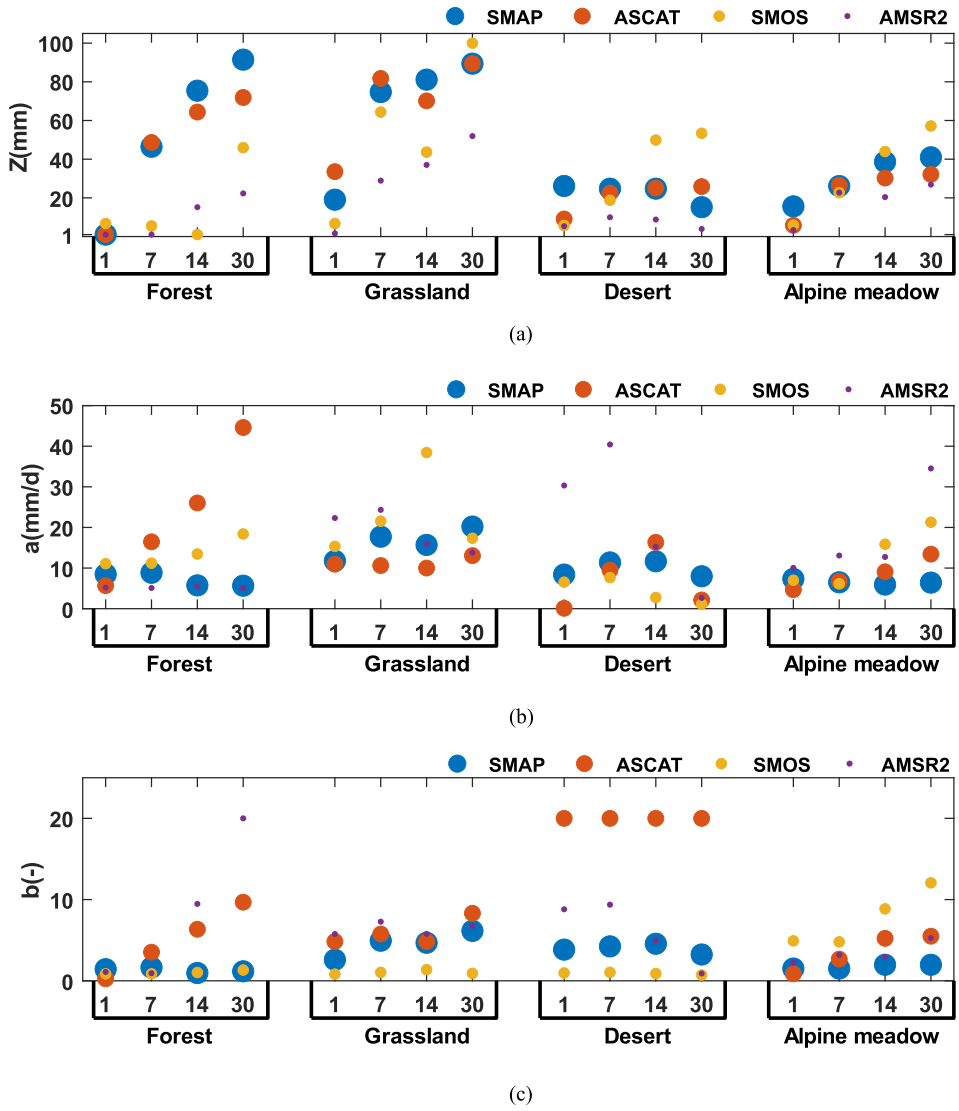

Fig. 7. Parameters Z, a, and b of SM2RAIN-SMAP, SM2RAIN-ASCAT, SM2RAIN-SMOS, and SM2RAIN-AMSR2 rainfall estimates under various land covers.

required, and additional ground observations are necessary for a comprehensive evaluation.

D. Assessment of Calibration Parameters in Land Covers

Fig. 7(a) depicts the variation of soil layer depth (Z) parameters under different land cover types (Forest, Desert, Alpine meadow, and Grassland) and soil moisture products (SMAP, ASCAT, SMOS, and AMSR2). Overall, the Z parameter exhibits a trend to gradually increase with rising AGGR, with this tendency slowing down at AGGR values of 14 and 30. However, the Z-value of SMOS accompanied with AGGR showed different rules in Forest and Grassland, which may be caused by the quality of soil moisture products of SMOS. Z-values are typically near 100 mm in forest and grassland areas and as low as 40 mm in the desert and alpine meadow regions. when AGGR reaches 30. While SMAP's Z-value is highest in forests, SMOS's Z-value is highest in grassland, desert, and Alpine meadow areas. The value of parameter Z depends on how humid the climate is; the more humid the climate, the higher the value of parameter Z [27]. This law is illustrated in the Z value changes for soil moisture products in SMAP, AMSR2, and ASCAT.

Figs. 5(c) and 7(b) depict variations in the parameter belonging to the saturated hydraulic conductivity (a) and pore size distribution related index (b) of areas with different types of land cover and soil moisture products. Under the Forest land cover, parameters a and b of ASCAT showed an increasing trend with the increase of AGGR. Parameters a and b of SMOS in Alpine meadow also showed a similar situation. The SMAP a and b parameters, out of the four soil moisture products, were the most stable and did not exhibit significant changes under various land cover types and AGGR values. These parameter values can be used as a guide for parameter sets in future investigations. The AMSR2 parameters a and b did not exhibit any clear patterns of fluctuation. Most of the parameters a varied mostly between 20 and 30, whereas parameter b varied between 10 and 15. However, the ASCAT b parameter showed greater values under the Desert land cover type, remaining generally consistent at

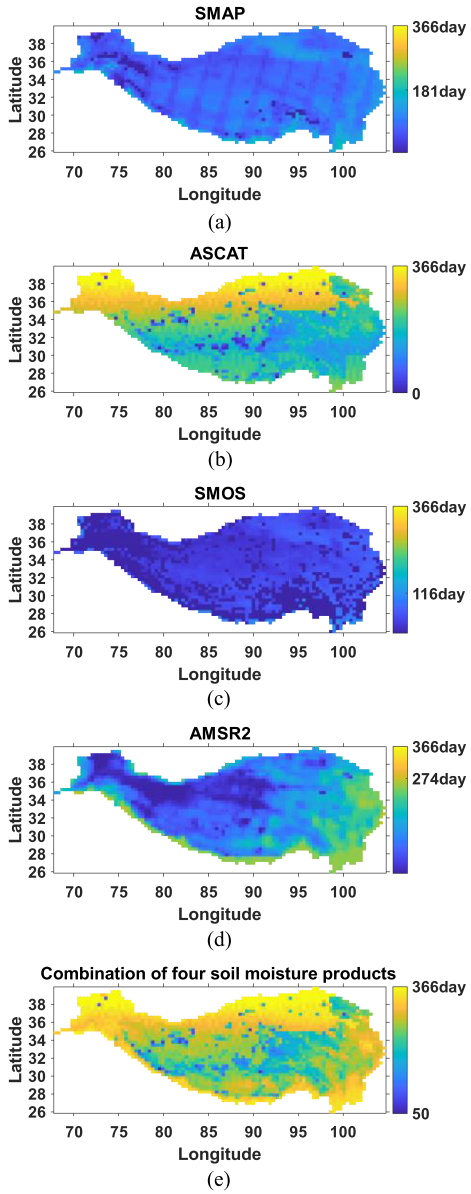

Fig. 8. Percentage of days with available SMAP, ASCAT, SMOS and AMSR2 soil moisture retrievals in 2016.

around 20, significantly higher than the parameter values of other soil moisture products.

V. Discussion

A. Spatial and Temporal Soil Moisture Completeness

To assess the temporal coverage of the four satellite soil moisture products on the Tibetan Plateau in 2016, ASCAT, SMOS, and AMSR2 were resampled to the EASE-2 Grid using the grid of SMAP products as a reference (see Fig. 8).

On the Tibetan Plateau, the SMAP soil moisture product has a very consistent temporal coverage, but a large number of missing data are produced because of the scanning gap in satellite observations. Particularly during the freezing period, just 181 of 366 days (50%) had reliable soil moisture data, which is virtually entirely missing values [see Fig. 8(a)]. In the northern Tibetan Plateau, ASCAT soil moisture products offer greater temporal coverage, with some grids even covering the entire year (including the soil freezing period) [see Fig. 8(b)]. With the highest temporal coverage grids only reaching 116 days (about 30%) [see Fig. 8(c)], the temporal coverage of SMOS soil moisture products in the Tibetan Plateau is significantly lower than that of other products, which is because SMOS in the Tibetan plateau region is severely impacted by RFI. The AMSR2 soil moisture product has high temporal coverage in the eastern Tibetan Plateau, with the highest coverage raster reaching 274 days (∼75%) [see Fig. 8(d)]. The central high-altitude region of the Tibetan Plateau has more noticeable missing values for the ASCAT, SMOS, and AMSR2 soil moisture products than any other location, which suggests that the high-altitude region has a greater influence on the acquisition of soil moisture. By combining the four soil moisture products, the combined soil moisture data's time coverage was significantly increased, and the grid with the lowest time coverage could reach 50 days [see Fig. 8(e)]. This finding indicates that various soil moisture data can complement one another and thereby significantly increase the frequency of soil moisture observations.

B. Comparison of SM2RAIN-Derived Rainfall Estimation Using Different Combined Soil Moisture Products

It can be seen from Section V-A that different satellite soil moisture products can complement each other to improve the temporal resolution of soil moisture over the Tibetan Plateau. In this section, we try to combine different soil moisture products by (6) and then use the DCT-PLS algorithm to fill the missing soil moisture to estimate rainfall. The experiment shows that the performance of rainfall estimation from combining several soil moisture products is inferior to that of a single soil moisture product after DCT-PLS filling (not shown here). Similarly, Saeedi et al. [71] recently demonstrated a similar situation when evaluating the SM2RAIN algorithm in the Lake Urmia basin, Iran, where the ASCAT soil moisture after DCT-PLS filling was significantly better than the combination of SMAP and ASCAT at an AGGR of 30 days, which may be due to the systems error of the various soil moisture product. To address the issue mentioned above, this section evaluates the performance of the SM2RAIN algorithm applied to each soil moisture product by first filling in the missing values using the DCT-PLS algorithm and then combining the soil moisture using (7).

It is evident from the study above that SMAP soil moisture has the best performance in estimating rainfall. To compare the performance of SMAP, SMAP+ASCAT, SMAP+SMOS, and SMAP+AMSR2 as input data for the SM2RAIN algorithm, the other three soil moisture data were combined with SMAP soil moisture independently (see Tables IV and V). When merging satellite soil moisture products, ASCAT and AMSR2 are subject to exponential filtering to make them more consistent with L band data (SMAP). It is important to note that we also attempted to combine three and four soil moisture products, but these combinations did not produce better results because it was challenging to determine the weight of each soil moisture

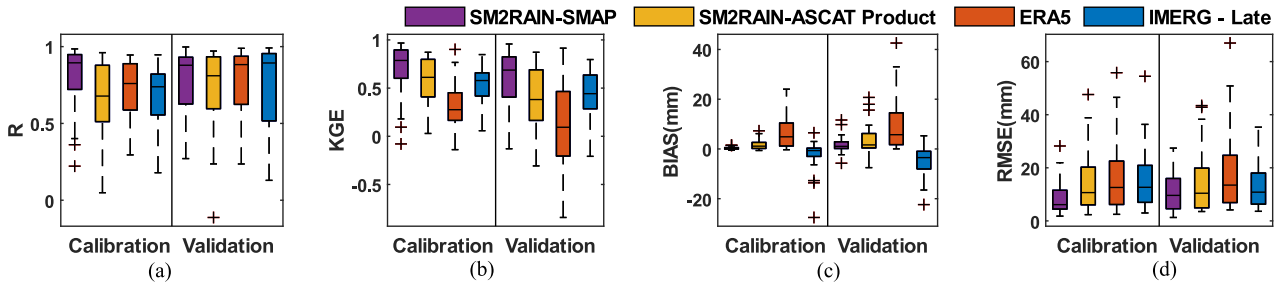

Fig. 9. Comparison of the performance of SM2RAIN-SMAP rainfall estimation, SM2RAIN-ASCAT rainfall product, ERA5 and IMERG-late satellite rainfall product in the AGGR of 17,14,30 days (R, KGE, BIAS, RMSE).

TABLE IV
EVALUATION METRIC R OF AGGR AT 1, 7, 14, AND 30 DAYS OF RAINFALL ESTIMATION FOR DIFFERENT COMBINATIONS

	Calibration				Validation			
SM product	1	7	14	30	1	7	14	30
SMAP	0.44	0.84	0.89	0.95	0.41	0.83	0.90	**0.95**
SMAP+ASCAT	**0.49**	**0.87**	**0.92**	0.96	**0.45**	**0.85**	**0.91**	0.94
SMAP+SMOS	0.46	0.86	0.91	0.96	0.40	0.84	0.89	0.92
SMAP+AMSR2	0.46	**0.87**	**0.92**	**0.97**	0.43	0.84	0.90	0.94
ESA CCI	0.39	0.81	0.88	0.95	0.41	0.81	0.88	0.93

Note: The maximum values in each column are underlined and bolded.

TABLE V
EVALUATION METRIC KGE OF AGGR AT 1, 7, 14, AND 30 DAYS OF RAINFALL ESTIMATION FOR DIFFERENT COMBINATIONS

	Calibration				Validation			
SM product	1	7	14	30	1	7	14	30
SMAP	0.21	0.75	0.81	0.89	0.14	0.67	0.77	0.80
SMAP+ASCAT	**0.29**	**0.79**	**0.86**	0.91	**0.17**	0.68	**0.79**	**0.85**
SMAP+SMOS	0.23	0.77	0.84	0.92	0.14	**0.69**	0.77	0.73
SMAP+AMSR2	0.24	0.78	0.84	**0.93**	**0.17**	**0.69**	0.74	0.79
ESA CCI	0.18	0.73	0.84	0.91	0.15	0.60	0.65	0.76

Note: The maximum values in each column are underlined and bolded.

product. For this reason, we will only discuss the scenario of combining two soil moisture products at a time.

All other combinations could somewhat enhance the performance of SM2RAIN, but the SMAP+ASCAT combination performed the best overall. At an AGGR of 17,14 days, the mean *R* of SMAP+ASCAT were superior to other combinations (calibration and validation periods), with an improvement in mean *R* of 1%–4% for the calibration period and 1%–4% for the validation period compared to SMAP. SMAP+AMSR2 had somewhat superior mean *R* for the calibration and validation periods at an AGGR of 30 days than did SMAP+ASCAT (see Table IV), but the performance gap between the various combinations was not very large.

Similarly, compared to SMAP, the combination of SMAP+ASCAT obtained a considerable improvement in the mean value of *KGE*, a 2%–8% improvement in the mean value of *R* in the calibration period, and a 1%–5% improvement in the validation period (see Table V). Based on these findings, it can be concluded that SMAP+ASCAT is the best combination option for maximizing the potential of the SM2RAIN algorithm by combining diverse soil moisture products.

In comparison to the outcomes achieved by combining the SMAP soil moisture product with the other three satellite soil moisture products, the utilization of the ESA CCI soil moisture product for rainfall estimation yielded unsatisfactory results (see Tables IV and V). Our analysis suggests that this discrepancy can be attributed to a significant systematic error arising from the ESA CCI soil moisture products using multisource soil moisture products. These findings indicate that the SM2RAIN algorithm may hold distinct advantages by employing a more robust gap filling algorithm instead of relying solely on multisource soil moisture merging techniques [71].

C. SM2RAIN-Derived Rainfall Estimation Versus Other Rainfall Products

It is clear from Section IV-B that SMAP soil moisture performs best when used as input data for the SM2RAIN algorithm. This section continues to use SM2RAIN-SMAP rainfall estimation as a representative and compares it with SM2RAIN-ASCAT, ERA5, and IMERG-Late rainfall at AGGR of 1, 7, 14, and 30, respectively (see Fig. 9). It is important to note that this

analysis was performed at the product level and therefore the SM2RAIN-ASCAT rainfall product did not use in situ rainfall data to calibrate the parameters, the SM2RAIN-SMAP rainfall estimates used ground observation for local calibration.

It is not surprising that the results of SM2RAIN-SMAP show the best performance, since SM2RAIN-SMAP is calibrated against the rain gauge (see Fig. 9). SM2RAIN-SMAP showed the highest correlation with rain gauges [see Fig. 9(a)]. The *KGE* of SM2RAIN-SMAP precipitation estimation is significantly higher than that of other precipitation products [see Fig. 9(b)], indicating that SM2RAIN-SMAP precipitation estimation has good robustness. For Bias, SM2RAIM-SMAP and SMARAIN-ASCAT products are closer to 0, showing good Bias performance [see Fig. 9(c)], which is due to the ability of SM2RAIN algorithm to continuously reproduce cumulative rainfall in the case of limited satellite transit times [29]. ERA5 significantly overestimated rainfall, while IMERG-Late significantly underestimated rainfall [see Fig. 9(c)]. As can be seen from the *RMSE*, SM2RAIN-SMAP shows the smallest error [see Fig. 9(d)]. The results show that SM2RAIN-SMAP has the best performance among the four rainfall estimates, which indicates the good potential of SMAP application in rainfall estimation over the Tibetan Plateau.

VI. Conclusion

This study evaluated the performance of various soil moisture products (SMAP, ASCAT, SMOS, and AMSR2) as input data to the SM2RAIN algorithm for rainfall estimation in the Tibetan Plateau region, and analyzes the performance of rainfall estimate in various land cover types. To further improve the effectiveness of the SM2RAIN method, the DCT-PLS algorithm was used to fill in the missing values of the soil moisture products and to attempt to combine various soil moisture products. The performance of the SM2RAIN method was further improved by combining various soil moisture products as input data and using the DCT-PLS algorithm to fill in the missing values of the soil moisture products. Finally, the SM2RAIN-SMAP rainfall data, the SM2RAIN-ASCAT rainfall product, the IMERG satellite rainfall product, and the ERA5 rainfall product were compared. Our main conclusions from this study can be summarized as follows:

1) SMAP, ASCAT, SMOS, and AMSR2 soil moisture products can achieve good rainfall estimation at the time aggregation scale in AGGR over 7 days (the mean *R* is between 0.74 and 0.84, The mean *KGE* is between 0.53 and 0.75). The performance of SMAP soil moisture estimation of rainfall is superior to that of the other rainfall products among the four soil moisture products.
2) Different soil moisture products can complement each other, with the combination of SMAP and ASCAT having more significant potential as an input data to the SM2RAIN algorithm.
3) The SM2RAIN-SMAP rainfall estimation is superior to the satellite rainfall product IMERG-Late and the reanalysis rainfall product ERA5.

In the future, we plan to develop more robust multisource soil moisture product combination algorithms and missing value filling algorithms to obtain spatio-temporal seamless soil moisture data, and using such soil moisture data is expected to further improve the accuracy of the SM2RAIN algorithm for rainfall estimation and increase its potential for rainfall estimation.

References

[1] L. Liang, L. Li, C. Liu, and L. Cuo, "Climate change in the Tibetan Plateau three rivers source region: 1960–2009," *Int. J. Climatol.*, vol. 33, no. 13, pp. 2900–2916, Nov. 2013, doi: 10.1002/joc.3642.

[2] K. Tong, F. Su, D. Yang, L. Zhang, and Z. Hao, "Tibetan Plateau precipitation as depicted by gauge observations, reanalyses and satellite retrievals," *Int. J. Climatol.*, vol. 34, no. 2, pp. 265–285, Feb. 2014, doi: 10.1002/joc.3682.

[3] P. Li et al., "Mesoscale convective system precipitation characteristics over East Asia. Part I: Regional differences and seasonal variations," *J. Climate*, vol. 33, no. 21, pp. 9271–9286, Nov. 2020, doi: 10.1175/JCLI-D-20-0072.1.

[4] X. Xia, Y. Liu, W. Jing, and L. Yao, "Assessment of four satellite-based precipitation products over the Pearl River Basin, China," *IEEE Access*, vol. 9, pp. 97729–97746, 2021.

[5] Q. Ge, J. Zheng, Z. Hao, Y. Liu, and M. Li, "Recent advances on reconstruction of climate and extreme events in China for the past 2000 years," *J. Geographical Sci.*, vol. 26, no. 7, pp. 827–854, 2016, doi: 10.1007/s11442-016-1301-4.

[6] S. Thaler, L. Brocca, L. Ciabatta, J. Eitzinger, S. Hahn, and W. Wagner, "Effects of different spatial precipitation input data on crop model outputs under a central European climate," *Atmosphere*, vol. 9, no. 8, 2018, Art. no. 290, doi: 10.3390/atmos9080290.

[7] Y. Hu et al., "Spatial and temporal variations in the rainy season onset over the Qinghai-Tibet Plateau," *Water*, vol. 11, no. 10, Oct. 2019, Art. no. 1960, doi: 10.3390/w11101960.

[8] E. Forootan et al., "Understanding the global hydrological droughts of 2003–2016 and their relationships with teleconnections," *Sci. Total Environ.*, vol. 650, pp. 2587–2604, 2019, doi: 10.1016/j.scitotenv.2018.09.231.

[9] B. Wang, Q. Bao, B. Hoskins, G. Wu, and Y. Liu, "Tibetan Plateau warming and precipitation changes in East Asia," *Geophys. Res. Lett.*, vol. 35, no. 14, pp. 1–5, 2008, doi: 10.1029/2008GL034330.

[10] J. Qin, K. Yang, S. Liang, and X. Guo, "The altitudinal dependence of recent rapid warming over the Tibetan Plateau," *Climatic Change*, vol. 97, no. 1, Art. no. 321, doi: 10.1007/s10584-009-9733-9.

[11] J.-S. Ye, J. F. Reynolds, G.-J. Sun, and F.-M. Li, "Impacts of increased variability in precipitation and air temperature on net primary productivity of the Tibetan Plateau: A modeling analysis," *Climatic Change*, vol. 119, no. 2, pp. 321–332, 2013, doi: 10.1007/s10584-013-0719-2.

[12] K. Yang, H. Wu, J. Qin, C. G. Lin, W. J. Tang, and Y. Y. Chen, "Recent climate changes over the Tibetan Plateau and their impacts on energy and water cycle: A review," *Glob. Planet. Change*, vol. 112, pp. 79–91, 2014, doi: 10.1016/j.gloplacha.2013.12.001.

[13] X. Jiang, Y. Li, S. Yang, J. Shu, and G. He, "Interannual variation of mid-summer heavy rainfall in the eastern edge of the Tibetan Plateau," *Climate Dyn.*, vol. 45, no. 11, pp. 3091–3102, 2015, doi: 10.1007/s00382-015-2526-0.

[14] Z. Zhou, F. Zhou, M. Zhang, B. Lei, and Z. Ma, "Effect of increasing rainfall on the thermal—Moisture dynamics of permafrost active layer in the central Qinghai—Tibet Plateau," *J. Mountain Sci.*, vol. 18, no. 11, pp. 2929–2945, 2021, doi: 10.1007/s11629-021-6707-5.

[15] G. Villarini, P. V. Mandapaka, W. F. Krajewski, and R. J. Moore, "Rainfall and sampling uncertainties: A rain gauge perspective," *J. Geophys. Res. Atmos.*, vol. 113, no. 11, pp. 1–12, 2008, doi: 10.1029/2007JD009214.

[16] P. Xu et al., "A two-phase copula entropy-based multiobjective optimization approach to hydrometeorological gauge network design," *J. Hydrol.*, vol. 555, pp. 228–241, Dec. 2017, doi: 10.1016/j.jhydrol.2017.09.046.

[17] C. Massari et al., "A daily 25 km short-latency rainfall product for data-scarce regions based on the integration of the global precipitation measurement mission rainfall and multiple-satellite soil moisture products," *Hydrol. Earth Syst. Sci.*, vol. 24, no. 5, pp. 2687–2710, May 2020, doi: 10.5194/hess-24-2687-2020.

[18] I. Paz, I. Tchiguirinskaia, and D. Schertzer, "Rain gauge networks' limitations and the implications to hydrological modelling highlighted with a X-band radar," *J. Hydrol.*, vol. 583, 2020, Art. no. 124615, doi: 10.1016/j.jhydrol.2020.124615.

[19] M. N. Khaliq, T. B. Ouarda, J. C. Ondo, P. Gachon, and B. Bobée, "Frequency analysis of a sequence of dependent and/or non-stationary hydro-meteorological observations: A review," *J. Hydrol.*, vol. 329, pp. 534–552, 2006.

[20] A. M. Ishak, R. Remesan, P. K. Srivastava, T. Islam, and D. Han, "Error correction modelling of wind speed through hydro-meteorological parameters and mesoscale model: A hybrid approach," *Water Resour. Manage.*, vol. 27, no. 1, pp. 1–23, Jan. 2013, doi: 10.1007/s11269-012-0130-1.

[21] D.-S. Shih, C.-H. Chen, and G.-T. Yeh, "Improving our understanding of flood forecasting using earlier hydro-meteorological intelligence," *J. Hydrol.*, vol. 512, pp. 470–481, May 2014, doi: 10.1016/j.jhydrol.2014.02.059.

[22] M. Suman and R. Maity, "Hybrid wavelet-ARX approach for modeling association between rainfall and meteorological forcings at river basin scale," *J. Hydrol.*, vol. 577, 2019, Art. no. 123918, doi: 10.1016/j.jhydrol.2019.123918.

[23] J. Fang, W. Yang, Y. Luan, J. Du, A. Lin, and L. Zhao, "Evaluation of the TRMM 3B42 and GPM IMERG products for extreme precipitation analysis over China," *Atmospheric Res.*, vol. 223, pp. 24–38, Jul. 2019, doi: 10.1016/j.atmosres.2019.03.001.

[24] P. Filippucci, L. Brocca, C. Massari, C. Saltalippi, W. Wagner, and A. Tarpanelli, "Toward a self-calibrated and independent SM2RAIN rainfall product," *J. Hydrol.*, vol. 603, 2021, Art. no. 126837, doi: 10.1016/j.jhydrol.2021.126837.

[25] L. Brocca, T. Moramarco, F. Melone, and W. Wagner, "A new method for rainfall estimation through soil moisture observations," *Geophys. Res. Lett.*, vol. 40, no. 5, pp. 853–858, Mar. 2013, doi: 10.1002/grl.50173.

[26] M. Saeedi, A. Sharafati, L. Brocca, and A. Tavakol, "Estimating rainfall depth from satellite-based soil moisture data: A new algorithm by integrating SM2RAIN and the analytical net water flux models," *J. Hydrol.*, vol. 610, 2022, Art. no. 127868, doi: 10.1016/j.jhydrol.2022.127868.

[27] L. Brocca et al., "Soil as a natural rain gauge: Estimating global rainfall from satellite soil moisture data," *J. Geophys. Res.*, vol. 119, no. 9, pp. 5128–5141, May 2014, doi: 10.1002/2014JD021489.

[28] L. Ciabatta et al., "SM2RAIN-CCI: A new global long-term rainfall data set derived from ESA CCI soil moisture," *Earth Syst. Sci. Data*, vol. 10, no. 1, pp. 267–280, Feb. 2018, doi: 10.5194/essd-10-267-2018.

[29] L. Brocca et al., "SM2RAIN-ASCAT (2007-2018): Global daily satellite rainfall data from ASCAT soil moisture observations," *Earth Syst. Sci. Data*, vol. 11, no. 4, pp. 1583–1601, 2019, doi: 10.5194/essd-11-1583-2019.

[30] S. Koohi, A. Azizian, and L. Brocca, "Spatiotemporal drought monitoring using bottom-up precipitation dataset (SM2RAIN-ASCAT) over different regions of Iran," *Sci. Total Environ.*, vol. 779, 2021, Art. no. 146535, doi: 10.1016/j.scitotenv.2021.146535.

[31] M. T. Brunetti, M. Melillo, S. Peruccacci, L. Ciabatta, and L. Brocca, "How far are we from the use of satellite rainfall products in landslide forecasting?," *Remote Sens. Environ.*, vol. 210, pp. 65–75, 2018, doi: 10.1016/j.rse.2018.03.016.

[32] A. Colliander et al., "Validation of SMAP surface soil moisture products with core validation sites," *Remote Sens. Environ.*, vol. 191, pp. 215–231, 2017, doi: 10.1016/j.rse.2017.01.021.

[33] Y. Qu et al., "Rebuilding a microwave soil moisture product using random forest adopting AMSR-E/AMSR2 brightness temperature and SMAP over the Qinghai–Tibet Plateau, China," *Remote Sens.*, vol. 11, no. 6, 2019, Art. no. 683, doi: 10.3390/rs11060683.

[34] J. Liu et al., "Evaluation of SMAP, SMOS-IC, FY3B, JAXA, and LPRM Soil moisture products over the Qinghai-Tibet Plateau and its surrounding areas," *Remote Sens.*, vol. 11, no. 7, 2019, Art. no. 792, doi: 10.3390/rs11070792.

[35] J. Tian et al., "Estimation of subsurface soil moisture from surface soil moisture in cold mountainous areas," *Hydrol. Earth Syst. Sci.*, vol. 24, no. 9, pp. 4659–4674, 2020, doi: 10.5194/hess-24-4659-2020.

[36] J. Zeng, Z. Li, Q. Chen, H. Bi, J. Qiu, and P. Zou, "Evaluation of remotely sensed and reanalysis soil moisture products over the Tibetan Plateau using in-situ observations," *Remote Sens. Environ.*, vol. 163, pp. 91–110, 2015, doi: 10.1016/j.rse.2015.03.008.

[37] Q. Wang, R. van der Velde, P. Ferrazzoli, X. Chen, X. Bai, and Z. Su, "Mapping soil moisture across the Tibetan Plateau plains using Aquarius active and passive L-band microwave observations," *Int. J. Appl. Earth Observ. Geoinf.*, vol. 77, pp. 108–118, 2019, doi: 10.1016/j.jag.2019.01.005.

[38] A. Tarpanelli, C. Massari, L. Ciabatta, P. Filippucci, G. Amarnath, and L. Brocca, "Exploiting a constellation of satellite soil moisture sensors for accurate rainfall estimation," *Adv. Water Resour.*, vol. 108, pp. 249–255, 2017, doi: 10.1016/j.advwatres.2017.08.010.

[39] W. Zhang, Y. Yi, J. S. Kimball, Y. Kim, and K. Song, "Climatic controls on spring onset of the Tibetan Plateau grasslands from 1982 to 2008," *Remote Sens.*, vol. 7, no. 12, pp. 16607–16622, Dec. 2015, doi: 10.3390/rs71215847.

[40] Z. Wei, Y. Meng, W. Zhang, J. Peng, and L. Meng, "Downscaling SMAP soil moisture estimation with gradient boosting decision tree regression over the Tibetan Plateau," *Remote Sens. Environ.*, vol. 225, pp. 30–44, 2019, doi: 10.1016/j.rse.2019.02.022.

[41] Z. Q. Chen, Q. Q. Shao, J. Y. Liu, and J. B. Wang, "Analysis of net primary productivity of terrestrial vegetation on the Qinghai-Tibet Plateau, based on MODIS remote sensing data," *Sci. China Earth Sci.*, vol. 55, no. 8, pp. 1306–1312, Aug. 2012, doi: 10.1007/s11430-012-4389-0.

[42] L. Zhu and P. Peng, *Meteorological Data of Surface Environment and Observation Network in China's Cold Region (2018)*. Beijing, China: Nat. Tibetan Plateau Data Center, 2020, doi: 10.11888/Meteoro.tpdc.270423.

[43] P. Zhang et al., "A dataset of 10-year regional-scale soil moisture and soil temperature measurements at multiple depths on the Tibetan Plateau," *Earth Syst. Sci. Data*, vol. 14, no. 12, pp. 5513–5542, 2022, doi: 10.5194/essd-14-5513-2022.

[44] A. Colliander et al., "Validation of soil moisture data products from the NASA SMAP mission," *IEEE J. Sel. Topics Appl. Earth Observ. Remote Sens.*, vol. 15, pp. 364–392, 2022, doi: 10.1109/JSTARS.2021.3124743.

[45] W. Wagner, G. Lemoine, and H. Rott, "A method for estimating soil moisture from ERS scatterometer and soil data," *Remote Sens. Environ.*, vol. 70, no. 2, pp. 191–207, 1999, doi: 10.1016/S0034-4257(99)00036-X.

[46] J. P. Wigneron et al., "SMOS-IC data record of soil moisture and L-VOD: Historical development, applications and perspectives," *Remote Sens. Environ.*, vol. 254, 2021, Art. no. 112238, doi: 10.1016/j.rse.2020.112238.

[47] H. Kim et al., "Global-scale assessment and combination of SMAP with ASCAT (active) and AMSR2 (passive) soil moisture products," *Remote Sens. Environ.*, vol. 204, pp. 260–275, 2018, doi: 10.1016/j.rse.2017.10.026.

[48] Q. Wu, H. Liu, L. Wang, and C. Deng, "Evaluation of AMSR2 soil moisture products over the contiguous United States using in situ data from the international soil moisture network," *Int. J. Appl. Earth Observ. Geoinf.*, vol. 45, pp. 187–199, 2016, doi: 10.1016/j.jag.2015.10.011.

[49] J. Du, J. S. Kimball, L. A. Jones, Y. Kim, J. Glassy, and J. D. Watts, "A global satellite environmental data record derived from AMSR-E and AMSR2 microwave Earth observations," *Earth Syst. Sci. Data*, vol. 9, no. 2, pp. 791–808, 2017, doi: 10.5194/essd-9-791-2017.

[50] A. Gruber, T. Scanlon, R. Van Der Schalie, W. Wagner, and W. Dorigo, "Evolution of the ESA CCI soil moisture climate data records and their underlying merging methodology," *Earth Syst. Sci. Data*, vol. 11, no. 2, pp. 717–739, 2019, doi: 10.5194/essd-11-717-2019.

[51] W. Dorigo et al., "ESA CCI soil moisture for improved Earth system understanding: State-of-the art and future directions," *Remote Sens. Environ.*, vol. 203, pp. 185–215, 2017, doi: 10.1016/j.rse.2017.07.001.

[52] H. Hersbach et al., "The ERA5 global reanalysis," *Quart. J. Roy. Meteorological Soc.*, vol. 146, no. 730, pp. 1999–2049, 2020, doi: 10.1002/qj.3803.

[53] G. J. Huffman, E. F. Stocker, D. T. Bolvin, E. J. Nelkin, and T. Jackson, "GPM IMERG early precipitation L3 half hourly 0.1 degree x 0.1 degree V06," Goddard Earth Sci. Data Inf. Services Center, Washington, DC, USA, 2019.

[54] J. S. Famiglietti and E. F. Wood, "Multiscale modeling of spatially variable water and energy balance processes," *Water Resour. Res.*, vol. 30, no. 11, pp. 3061–3078, 1994, doi: 10.1029/94WR01498.

[55] D. Garcia, "Robust smoothing of gridded data in one and higher dimensions with missing values," *Comput. Statist. Data Anal.*, vol. 54, no. 4, pp. 1167–1178, 2010, doi: 10.1016/j.csda.2009.09.020.

[56] G. Wang, D. Garcia, Y. Liu, R. de Jeu, and A. J. Dolman, "A three-dimensional gap filling method for large geophysical datasets: Application to global satellite soil moisture observations," *Environ. Model. Softw.*, vol. 30, pp. 139–142, 2012, doi: 10.1016/j.envsoft.2011.10.015.

[57] H. T. Pham, S. Kim, L. Marshall, and F. Johnson, "Using 3D robust smoothing to fill land surface temperature gaps at the continental scale," *Int. J. Appl. Earth Observ. Geoinf.*, vol. 82, 2019, Art. no. 101879, doi: 10.1016/j.jag.2019.05.012.

[58] C. S. Draper, J. P. Walker, P. J. Steinle, R. A. M. de Jeu, and T. R. H. Holmes, "An evaluation of AMSR-E derived soil moisture over Australia," *Remote Sens. Environ.*, vol. 113, no. 4, pp. 703–710, 2009, doi: 10.1016/j.rse.2008.11.011.

[59] W. Wagner et al., "The ASCAT soil moisture product: A review of its specifications, validation results, and emerging applications," *Meteorologische Zeitschrift*, vol. 22, no. 1, pp. 5–33, 2013, doi: 10.1127/0941-2948/2013/0399.

[60] J. Ma, J. Zhou, F. M. Gottsche, S. Liang, S. Wang, and M. Li, "A global long-term (1981-2000) land surface temperature product for NOAA AVHRR," *Earth Syst. Sci. Data*, vol. 12, no. 4, pp. 3247–3268, 2020, doi: 10.5194/essd-12-3247-2020.
[61] Y. Lai, J. Tian, W. Kang, C. Gao, W. Hong, and C. He, "Rainfall estimation from surface soil moisture using SM2RAIN in cold mountainous areas," *J. Hydrol.*, vol. 606, 2022, Art. no. 127430, doi: 10.1016/j.jhydrol.2022.127430.
[62] L. Miao, Z. Wei, Y. Zhong, and Z. Duan, "Improving the SM2RAIN-derived rainfall estimation using Bayesian optimization," *J. Hydrol.*, vol. 622, 2023, Art. no. 129728, doi: 10.1016/j.jhydrol.2023.129728.
[63] Q. Zhang, Q. Yuan, J. Li, Y. Wang, F. Sun, and L. Zhang, "Generating seamless global daily AMSR2 soil moisture (SGD-SM) long-term products for the years 2013-2019," *Earth Syst. Sci. Data*, vol. 13, no. 3, pp. 1385–1401, 2021, doi: 10.5194/essd-13-1385-2021.
[64] T. Zhao et al., "Soil moisture experiment in the Luan River supporting new satellite mission opportunities," *Remote Sens. Environ.*, vol. 240, 2020, Art. no. 111680.
[65] L. Zhao et al., "The scale-dependence of SMOS soil moisture accuracy and its improvement through land data assimilation in the central Tibetan Plateau," *Remote Sens. Environ.*, vol. 152, pp. 345–355, 2014, doi: 10.1016/j.rse.2014.07.005.
[66] H. Ma, J. Zeng, N. Chen, X. Zhang, M. H. Cosh, and W. Wang, "Satellite surface soil moisture from SMAP, SMOS, AMSR2 and ESA CCI: A comprehensive assessment using global ground-based observations," *Remote Sens. Environ.*, vol. 231, 2019, Art. no. 111215, doi: 10.1016/j.rse.2019.111215.
[67] J. Zheng et al., "Assessment of 24 soil moisture datasets using a new in situ network in the Shandian River Basin of China," *Remote Sens. Environ.*, vol. 271, 2022, Art. no. 112891, doi: 10.1016/j.rse.2022.112891.
[68] Y. Chen et al., "Evaluation of SMAP, SMOS, and AMSR2 soil moisture retrievals against observations from two networks on the Tibetan Plateau," *J. Geophys. Res.*, vol. 122, no. 11, pp. 5780–5792, 2017, doi: 10.1002/2016JD026388.
[69] A. Tavakol, V. Rahmani, S. M. Quiring, and S. V. Kumar, "Evaluation analysis of NASA SMAP L3 and L4 and SPoRT-LIS soil moisture data in the United States," *Remote Sens. Environ.*, vol. 229, pp. 234–246, 2019, doi: 10.1016/j.rse.2019.05.006.
[70] G. Portal et al., "Assessment of multi-scale SMOS and SMAP soil moisture products across the Iberian Peninsula," *Remote Sens.*, vol. 12, no. 3, pp. 1–19, 2020, doi: 10.3390/rs12030570.
[71] M. Saeedi, H. Kim, S. Nabaei, L. Brocca, V. Lakshmi, and H. Mosaffa, "A comprehensive assessment of SM2RAIN-NWF using ASCAT and a combination of ASCAT and SMAP soil moisture products for rainfall estimation," *Sci. Total Environ.*, vol. 838, 2022, Art. no. 156416, doi: 10.1016/j.scitotenv.2022.156416.

Linguang Miao received the B.S. degree in surveying and mapping engineering from the School of Surveying and Urban Spatial Information, Henan University of Urban Construction, Pingdingshan, China, in 2021. He is currently working toward the M.S. degree in photogrammetry and remote sensing with the School of Surveying and Land Information Engineering, Henan Polytechnic University, Jiaozuo, China.

His research interests include hydrological remote sensing and machine learning.

Zushuai Wei received the Ph.D. degree in photogrammetry and remote sensing from Wuhan University, Wuhan, China, in 2019.

He is currently an Assistant Professor with Jianghan University, Wuhan, China. His research interests include microwave remote sensing of soil moisture and its downscaling.

Fengmin Hu received the Ph.D. degree in photogrammetry and remote sensing from Wuhan University, Wuhan, China, in 2021.

Her research interests include microwave remote sensing of soil moisture downscaling and data fusion at the L-band.

Zheng Duan received the M.S. degree in cartography and GIS from the Graduate University of Chinese Academy of Sciences, Beijing, China, in 2010, and the Ph.D. degree in remote sensing and hydrological model from Delft University of Technology, Delft, The Netherlands, in 2014.

He was a Scientific Consultant with several institutes including UNESCO-IHE, Delft, The Netherlands, in the field of satellite-based estimation of actual evapotranspiration, soil moisture and biomass production, and land cover classification. Since July 2015, he has been an Assistant Professor with the Technische Universität München, München, Germany. His research interests include integration of remote sensing in hydrological model and water balance studies of lakes and catchments, satellite-based precipitation, evapotranspiration, and open water evaporation estimation.